

Supplementary Information for

Slow-down of the global natural vegetation greening trend with further rising atmospheric CO₂

Winkler et al.

Corresponding Author: Alexander J. Winkler.
E-mail: alexander.winkler@mpimet.mpg.de

This PDF file includes:

Figs. S1 to S16
Tables S1 to S3
References for SI reference citations

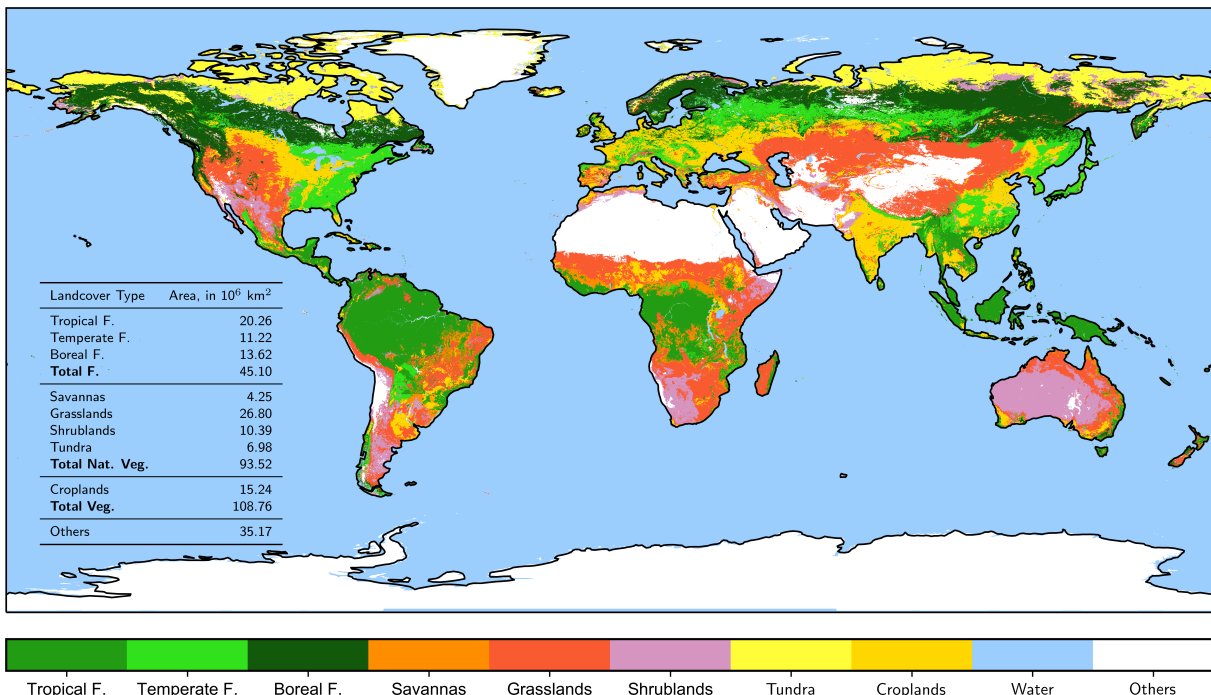


Fig. S1. Land cover map for broad vegetation classes. Global map of the distribution of broad land cover types based on the International Geosphere-Biosphere Programme (IGBP) classification, aggregated in anthropogenic (Croplands) and seven natural vegetation classes (Tropical, Temperate, and Boreal Forests, Savannas, Grasslands, Shrublands, and Tundra). The inset table shows the areal extent of each land cover type. Supplementary Table 1 provides a detailed overview on the conflation of the three land and forest cover products used to develop this map. Further details are depicted in the Materials and Methods section of the main paper.

Table S1. Scheme for mapping land covers used in this study from the International Geosphere-Biosphere Programme (IGBP) classes provided by MODIS (https://lpdaac.usgs.gov/dataset_discovery/modis/modis_products_table/mcd12c1_v006) and classes from Global Land Data Assimilation System (GLDAS; 1). MODIS tree cover product (https://lpdaac.usgs.gov/dataset_discovery/modis/modis_products_table/mod44b_v006) was used to account for the underestimated forested area in MODIS land cover product. Further details are depicted in Materials and Methods section of the main paper.

IGBP Land Cover Type	Land Cover This Study
Evergreen Needleleaf Forests (ENF)	Boreal Forest
Evergreen Broadleaf Forests (EBF)	Tropical Forest
Deciduous Needleleaf Forests (DNF)	Boreal Forest
Deciduous Broadleaf Forests (DBF)	Temperate Forest
Mixed Forests (MF)	Temperate Forest
Closed Shrublands	Shrublands
	Tropical Forests for tree cover > 20% and 25° S – 25° N
	Boreal Forests for tree cover > 10% and > 50° N/S
Open Shrublands	Shrublands
	Tundra for Wooded, Mixed or Bare Ground Tundra in GLDAS
	Tropical Forests for tree cover > 20% and 25° S – 25° N
	Boreal Forests for tree cover > 10% and > 50° N/S
Woody Savannas	1. Step: Tropical Forests for 25° S – 25° N 2. Step: Temperate Forests for DBF or MF in GLDAS Boreal Forests for ENF or DNF in GLDAS 3. Step: Temperate Forests for 25° N/S – 50° N/S Boreal Forests for > 50° N/S
Savannas	Savannas
	Croplands for Croplands in GLDAS
	Grasslands for Grasslands in GLDAS
	Shrublands for Open or Closed Shrublands in GLDAS
	Tropical Forests for tree cover > 20% and 25° S – 25° N
	Boreal Forests for tree cover > 10% and > 50° N/S
Grasslands	Grasslands
	Tundra for Wooded, Mixed or Bare Ground Tundra in GLDAS
	Tropical Forests for tree cover > 20% and 25° S – 25° N
	Boreal Forests for tree cover > 10% and > 50° N/S
Permanent Wetlands	Others
	Tundra for Wooded, Mixed or Bare Ground Tundra in GLDAS
Croplands	Croplands
Urban and Built-up Lands	Others
Cropland/Natural Vegetation Mosaics	Croplands
Permanent Snow and Ice	Others
Barren	Others
	Tundra for Wooded, Mixed or Bare Ground Tundra in GLDAS
Water Bodies	Water

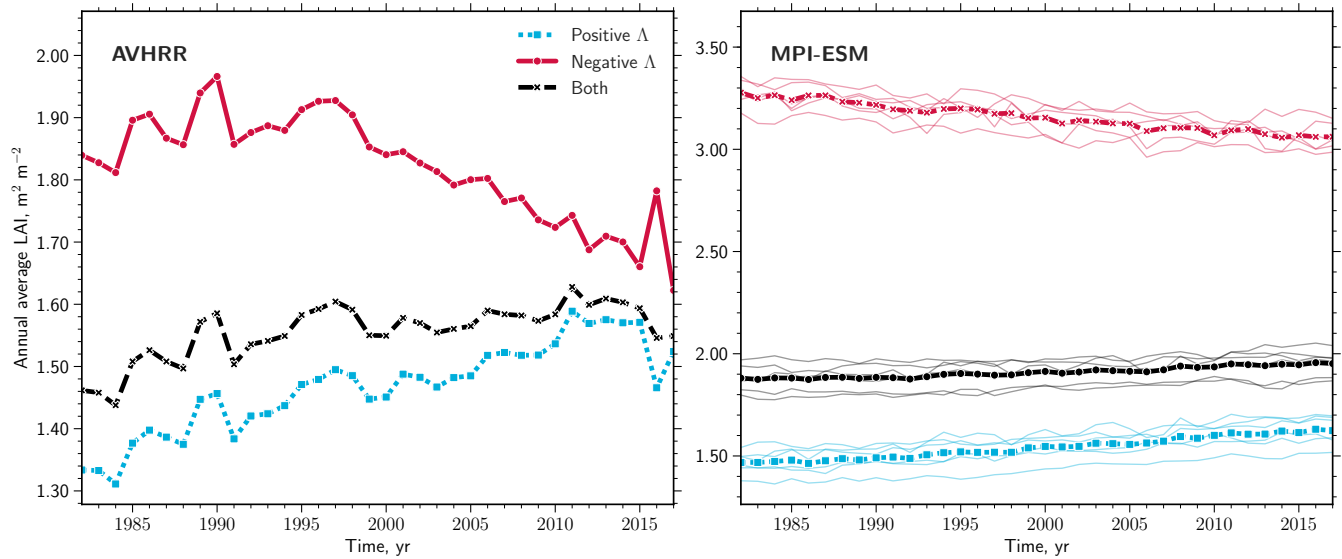


Fig. S2. Observations versus MPI-ESM ensemble. Time series of area-weighted annual average LAI (left: AVHRR, right: MPI-ESM) for regions exhibiting positive (blue line) and negative trends (red line) masked for natural vegetation (denoted Λ). Black lines represent the overall signal of all pixels. The individual MPI-ESM realizations are represented as thin lines and the ensemble means are shown in bold lines.

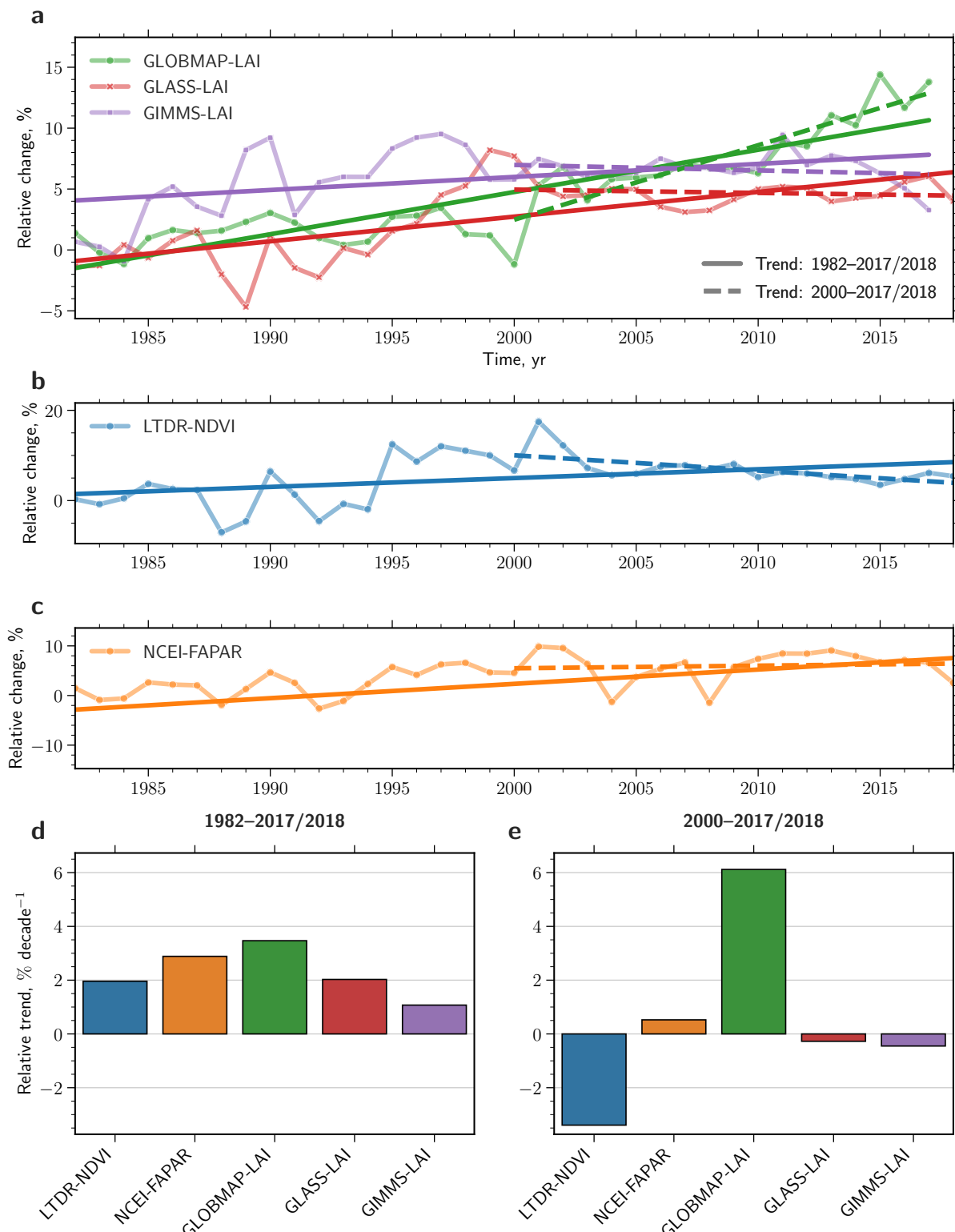


Fig. S3. Five different remote sensing datasets displaying the development of the natural vegetation over the last four decades. **a** Time series of changes in LAI relative to the average state from 1982–1984 as depicted in three different datasets (green: GLOBMAP-LAI, red: GLASS-LAI, and purple: GIMMS-LAI; see Materials and Methods section of the main paper for further details). The solid straight line represents the best linear fit for the entire period (1982–2017/2018), the dashed line represents the best linear fit for the second half of the period (2000–2017/2018). **b** as in **a** but for the dataset LTDR-NDVI (blue; see Materials and Methods section of the main paper for further details). **c** as in **a** but for the dataset NCEI-FAPAR (orange; see Materials and Methods section of the main paper for further details). **d** Bar chart comparing relative trends (in $\% \text{ decade}^{-1}$) in LAI, NDVI and FAPAR from different datasets for the entire period (1982–2017/2018) obtained from the gradients shown in **a-c**, respectively. **e** as in **d** but for the second half of the period (2000–2017/2018)

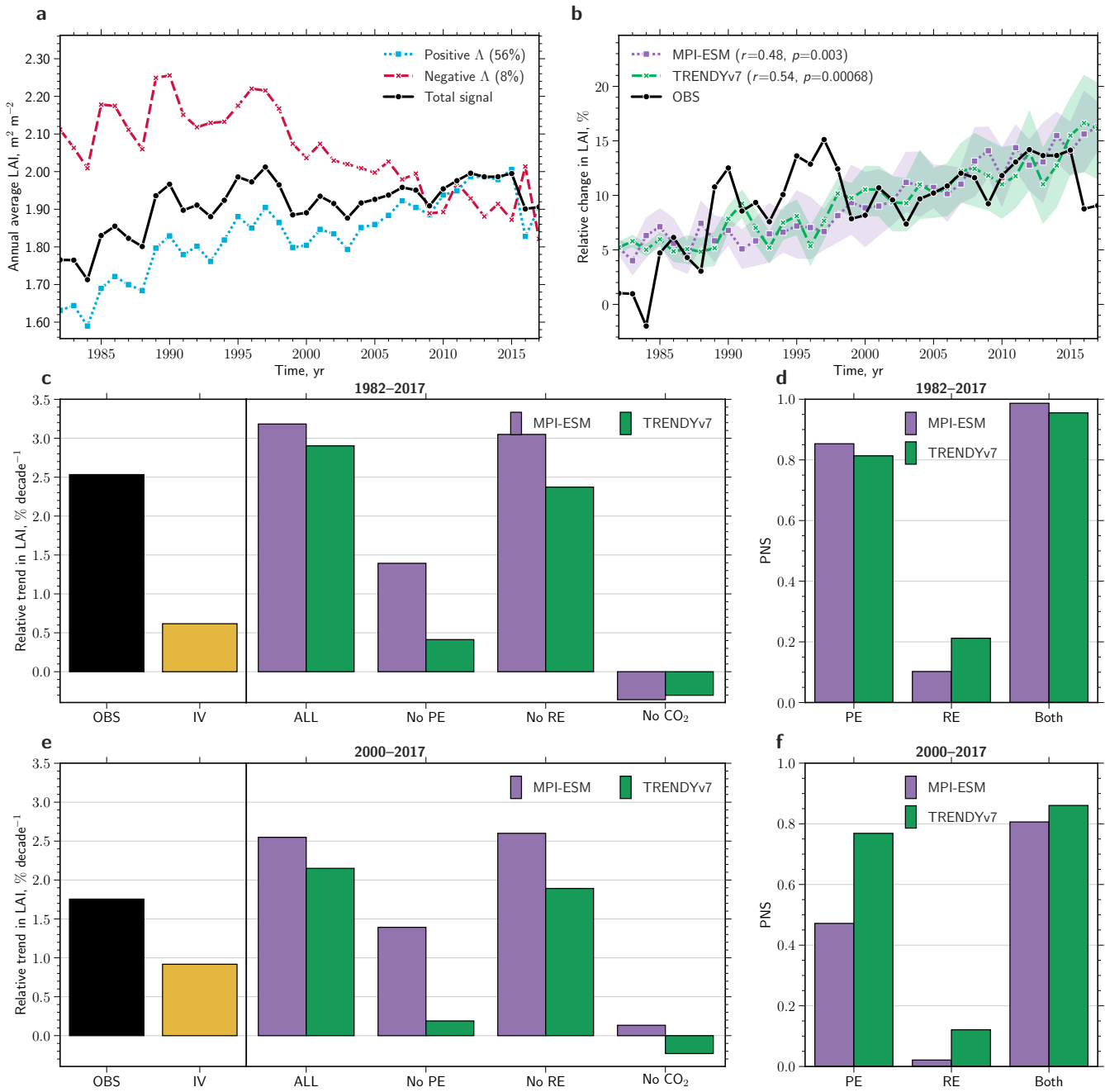


Fig. S4. Temperate Forests: Driver attribution of changing vegetation for the entire period versus the second half of the observational record. **a** Time series of the area-weighted annual average LAI (AVHRR, 1982–2017) for regions exhibiting increasing (blue dotted line) and decreasing LAI trends (red dashed line) of natural vegetation (Λ). The black solid line represents the overall signal of all pixels. The percentages in brackets in the legend represent the greening and browning proportions with respect to the total area. **b** Time series of changes in LAI relative to the average state from 1982–1984, comparing observations (black solid line) with historical simulations, where the green dashed line denotes the ensemble mean of 13 offline-driven land surface models (TRENDYv7, Materials and Methods), and the purple dotted line denotes the average of an ensemble of multi-realizations with a fully-coupled Earth system model (MPI-ESM, Materials and Methods). The colored shading represents the 95% confidence interval estimated by bootstrapping. The correlation coefficients (including significance level) of the observed and simulated time series are displayed in brackets in the legend. **c** Bar chart showing relative trends in LAI (in $\% \text{ yr}^{-1}$) of the total observed signal (black) and for factual (all historical forcings; ALL) as well as for counterfactual simulations, i.e. no historical CO_2 forcing (No CO_2), all historical forcings except the physiological effect (No PE) or the radiative effect (No RE) of atmospheric CO_2 , as estimated by TRENDYv7 (green) and MPI-ESM (purple). The yellow bar represents internal variability (IV) derived from all simulations (control, factual and counterfactual). **d** Probabilities of necessary and sufficient causation (PNS) of the change in LAI, comparing the physiological (PE) and radiative effect (RE) of CO_2 as well as their combined effect (Both). **e** as in **c** but for the period 2000–2017. **f** as in **d** but for the period 2000–2017.

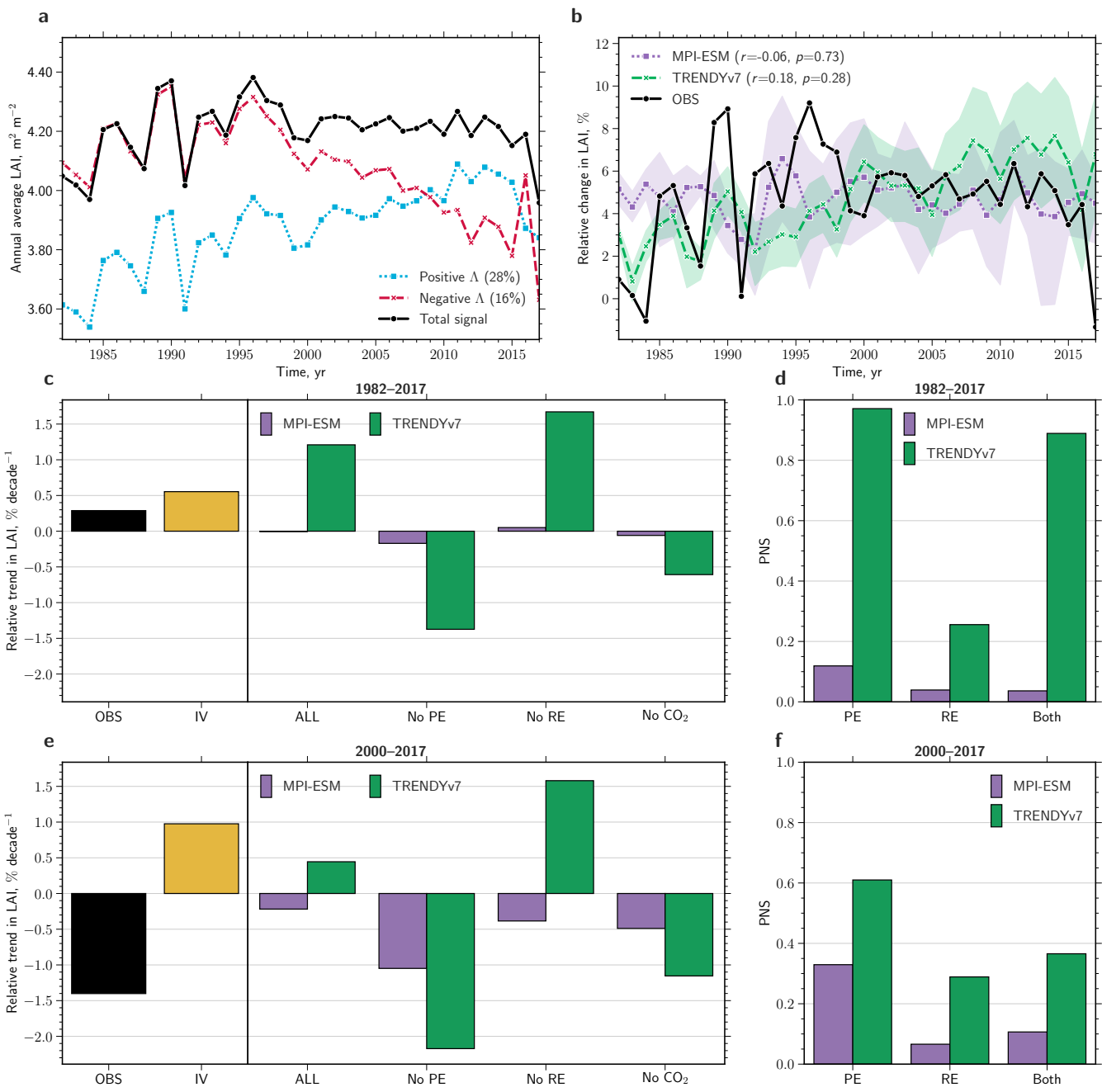


Fig. S5. Tropical Forests – caption analogous to Figure S4.

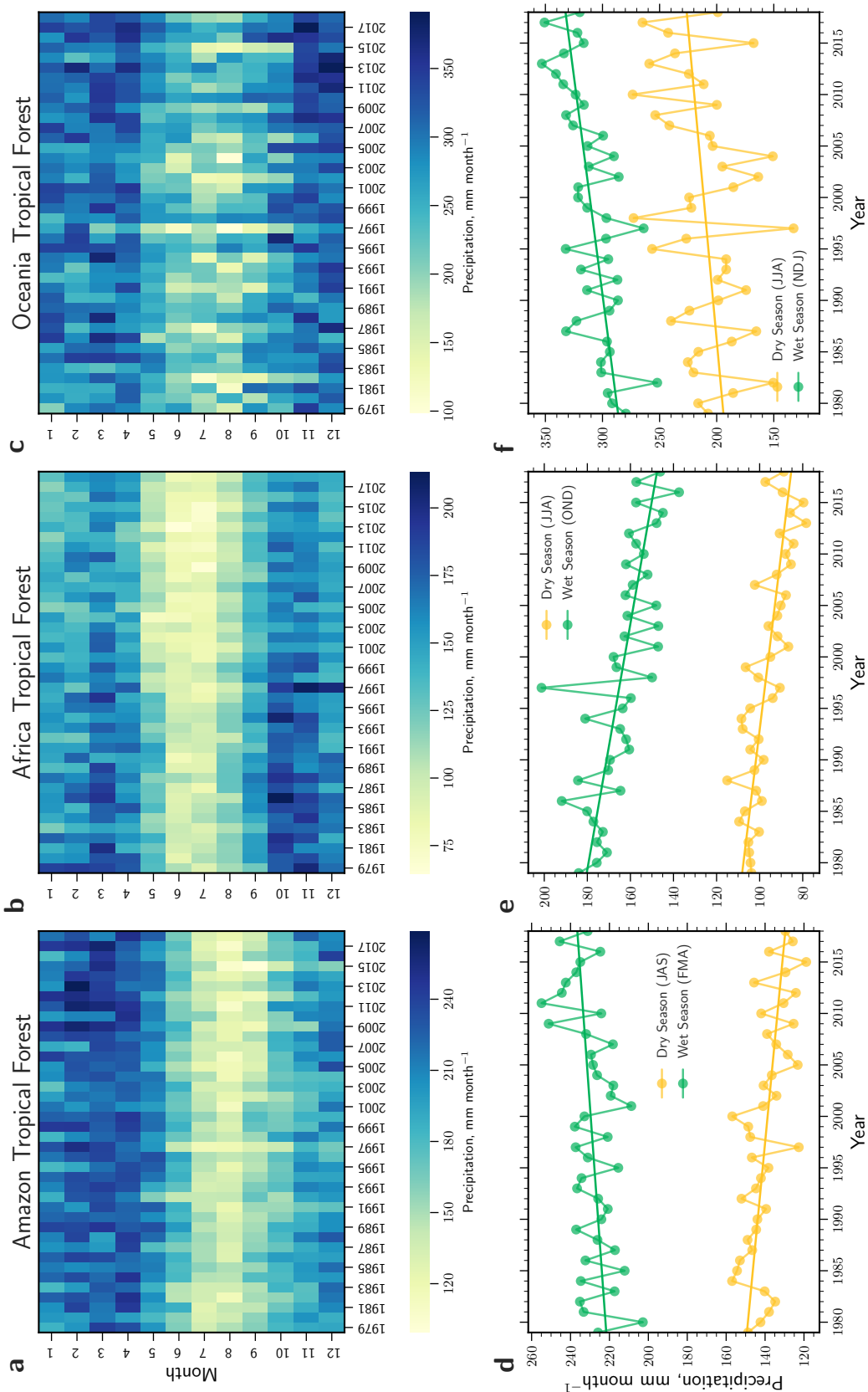


Fig. S6. Long-term precipitation changes in Tropical Forests. **a** Seasonality of monthly precipitation (from ECMWF ERA5, 2) throughout the satellite era (1979–2018) in tropical forests in the Amazon illustrated in a heat map, where colors indicate the intensity of rainfall. **b** and **c** as in **a**, but for tropical forests in Africa and Oceania, respectively. **d** Time series of mean monthly precipitation during dry (yellow line) and wet (green line) season in tropical forests in the Amazon, where the slopes represent the best linear fits. **e** and **f** as in **d**, but for tropical forests in Africa and Oceania, respectively. This analysis was performed using the Earth System Data Lab (3).

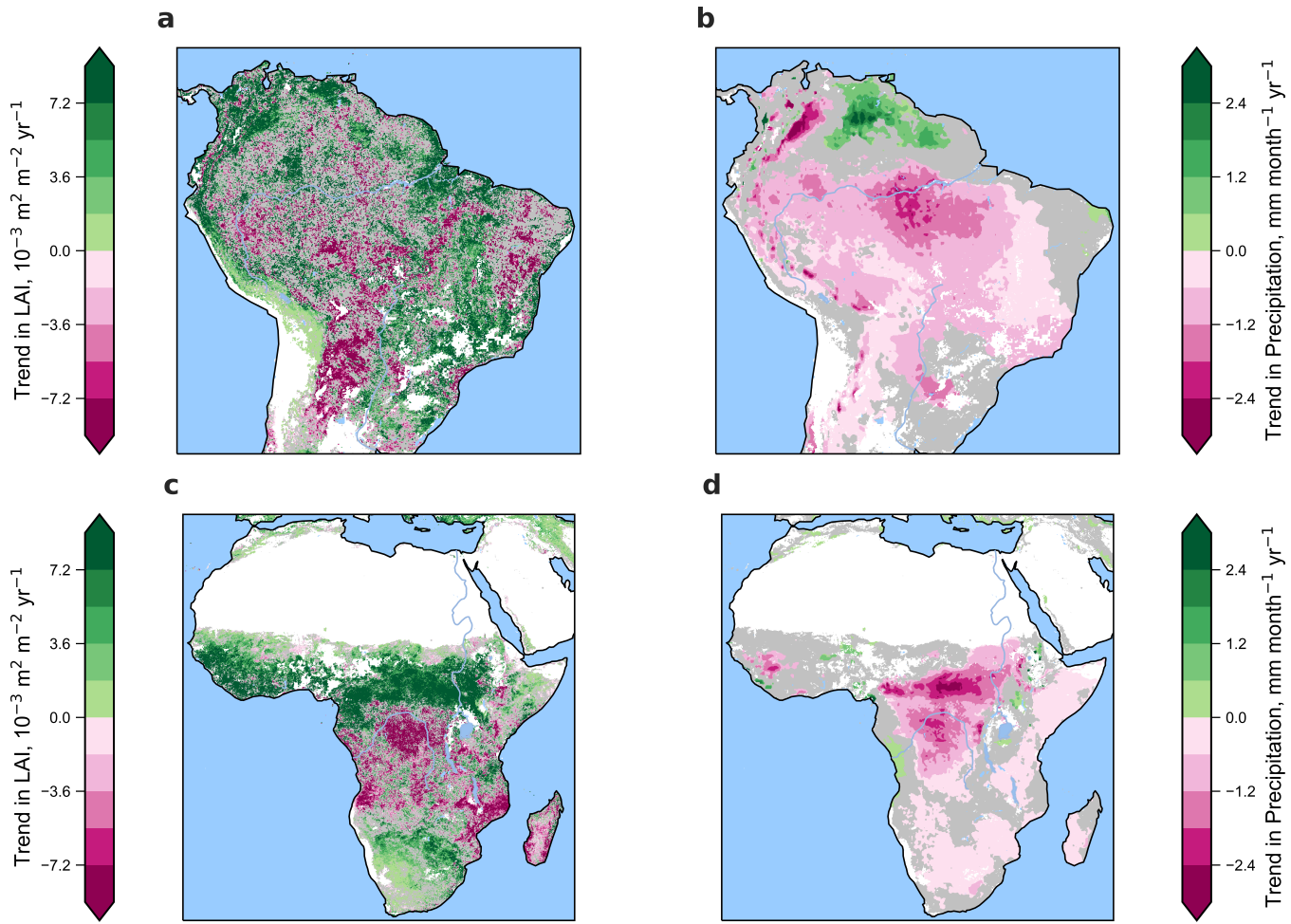


Fig. S7. Regional maps of trends in LAI and precipitation in Tropical Forests. **a, b** Statistically significant trends in annual average LAI (AVHRR) and in dry season precipitation in the Amazon (July – September) and **c, d** for Africa (June – August). Statistical significance is assessed using the Mann-Kendall test ($p < 0.1$). This analysis was performed using the Earth System Data Lab (3).

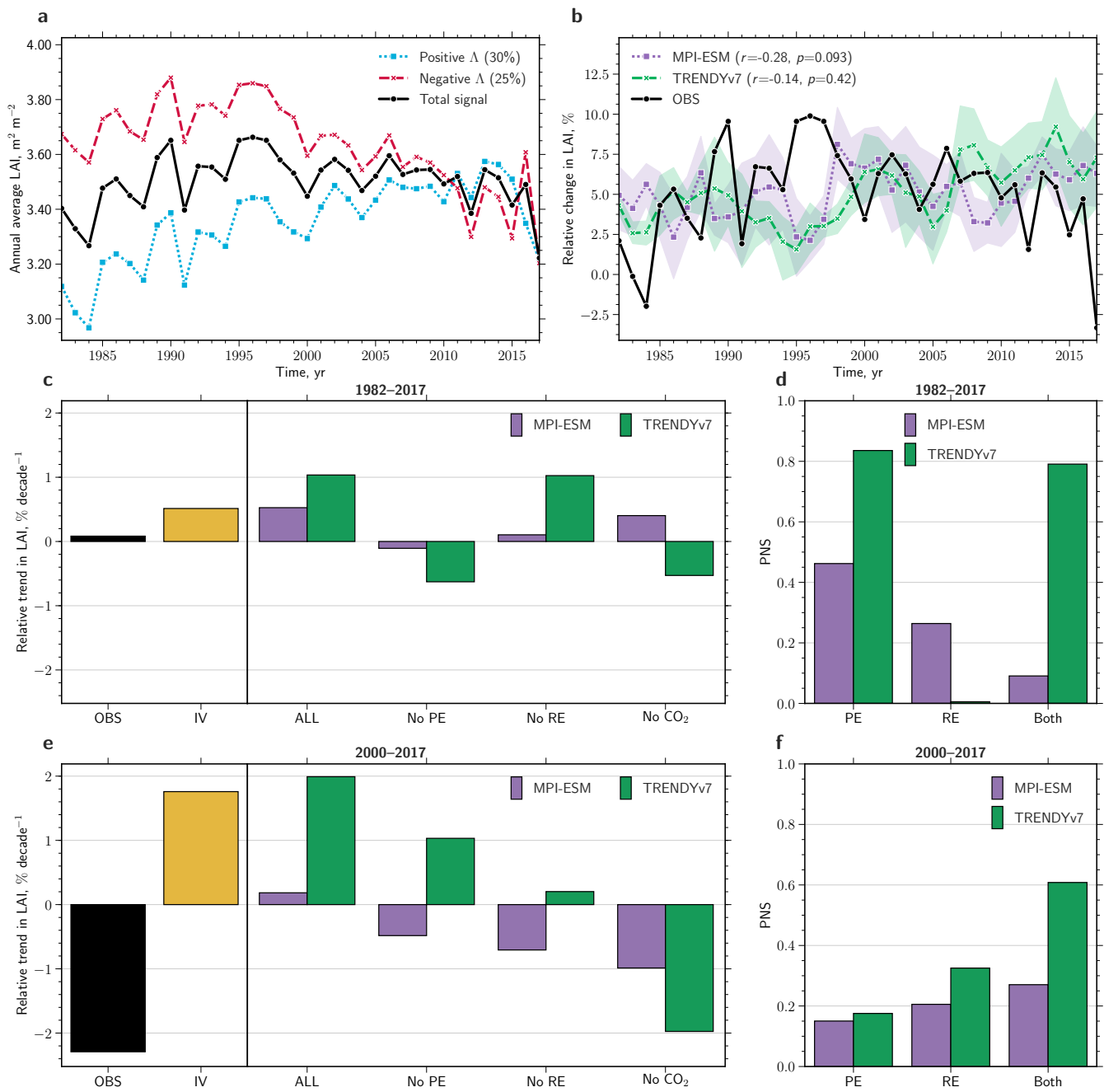


Fig. S8. Central African Tropical Forests – caption analogous to Figure S4.

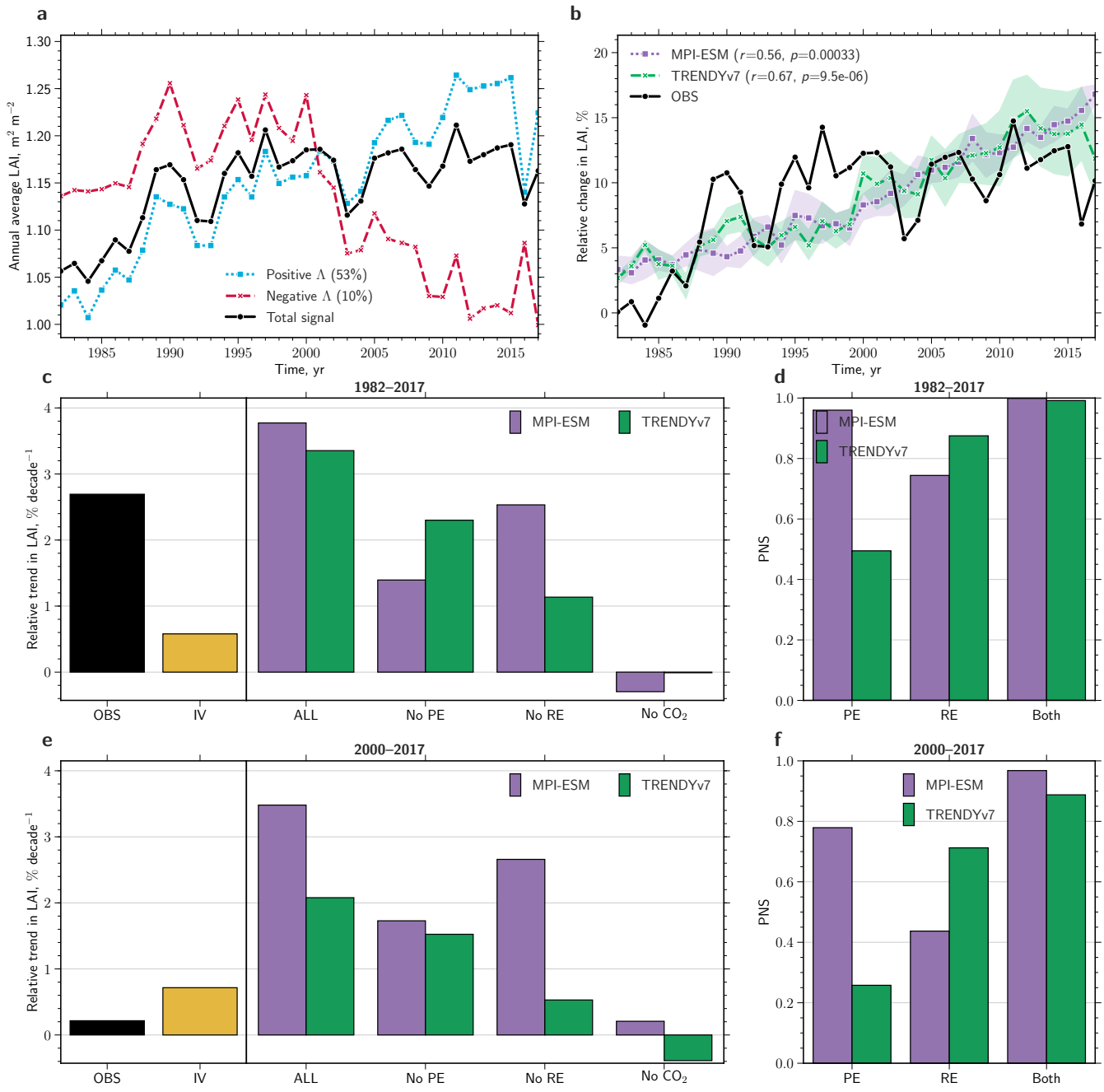


Fig. S9. Eurasian Boreal Forests – caption analogous to Figure S4.

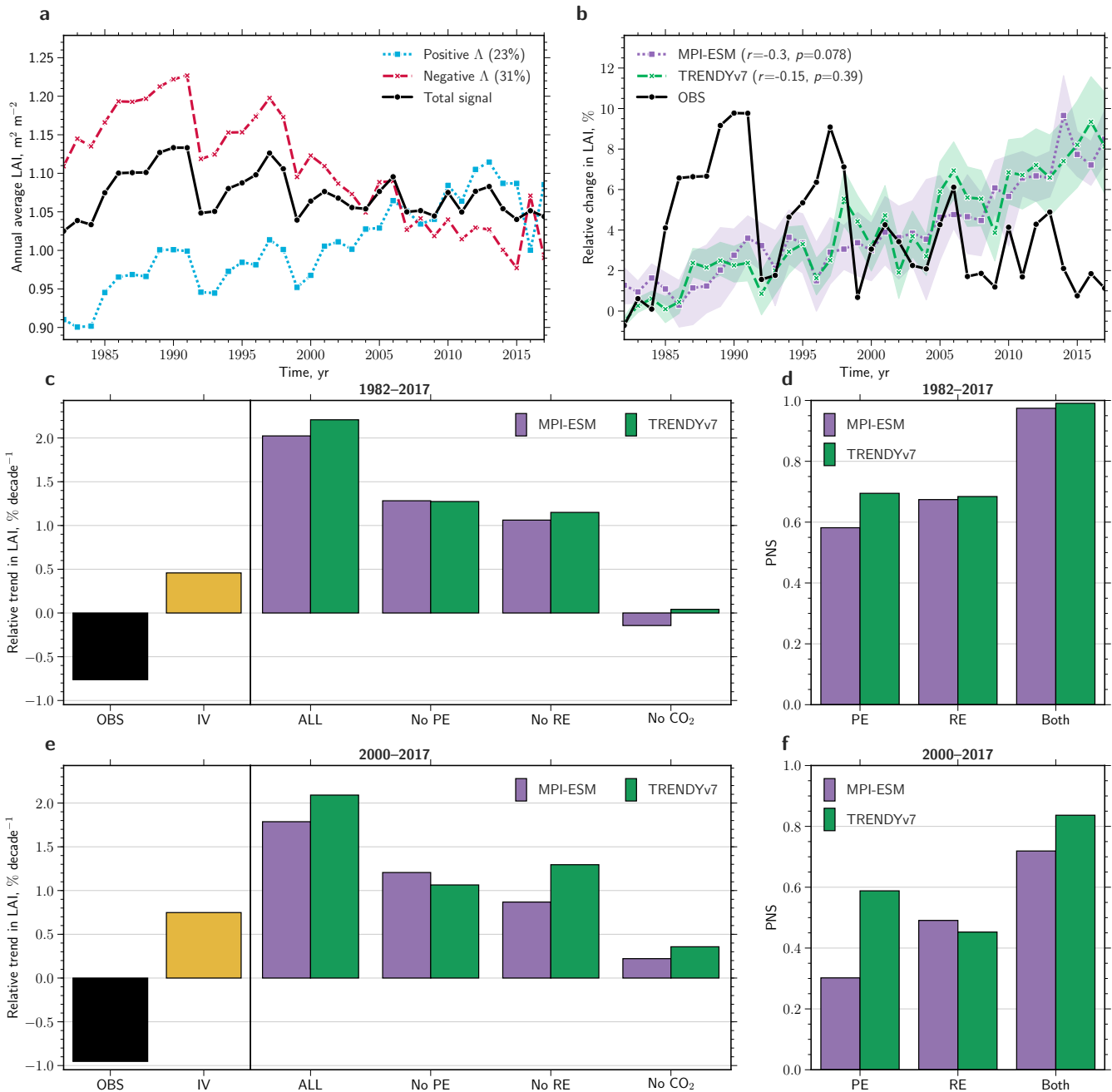


Fig. S10. North American Boreal Forests – caption analogous to Figure S4.

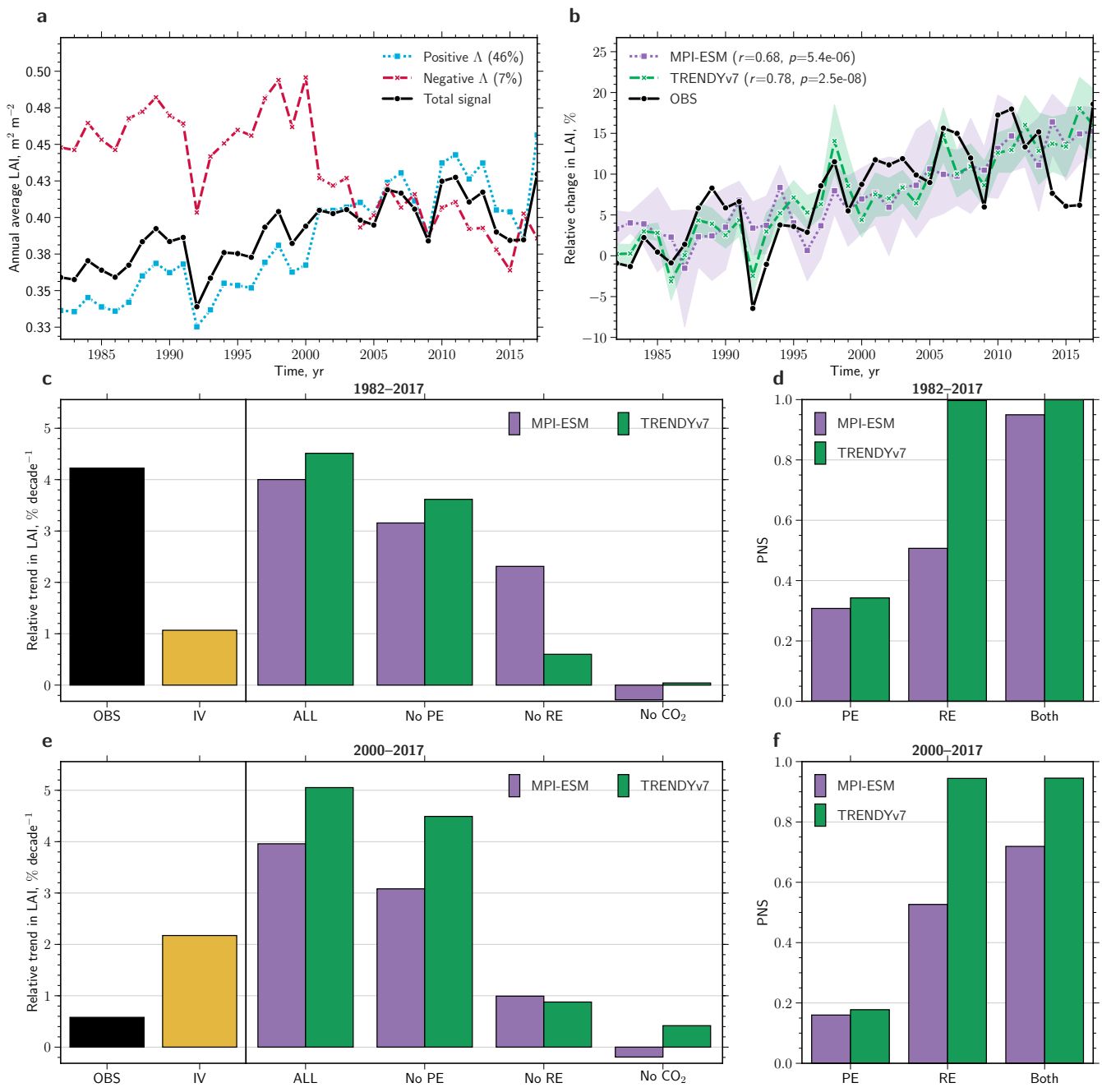


Fig. S11. North American Tundra – caption analogous to Figure S4.

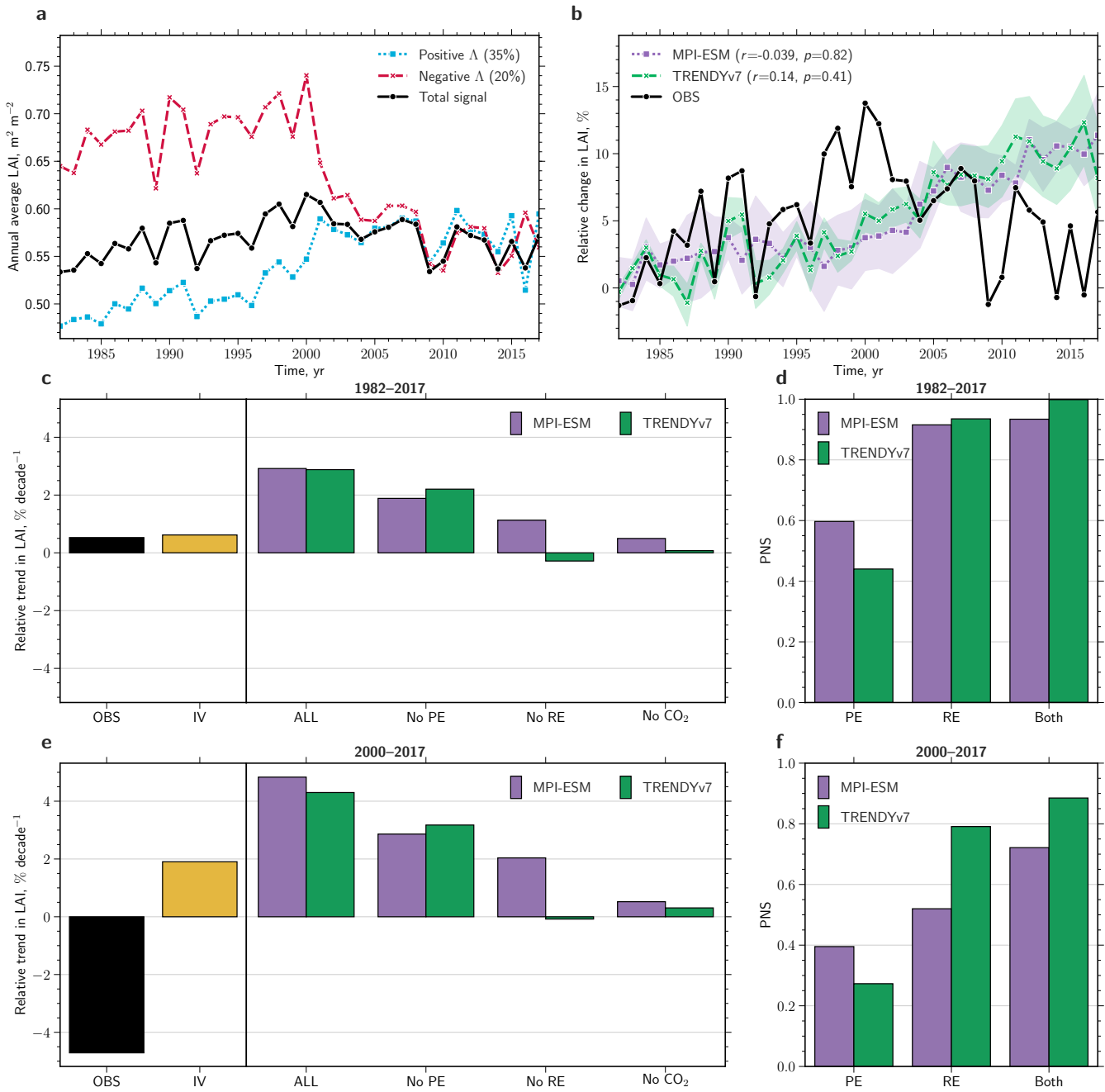


Fig. S12. Eurasian Tundra – caption analogous to Figure S4.

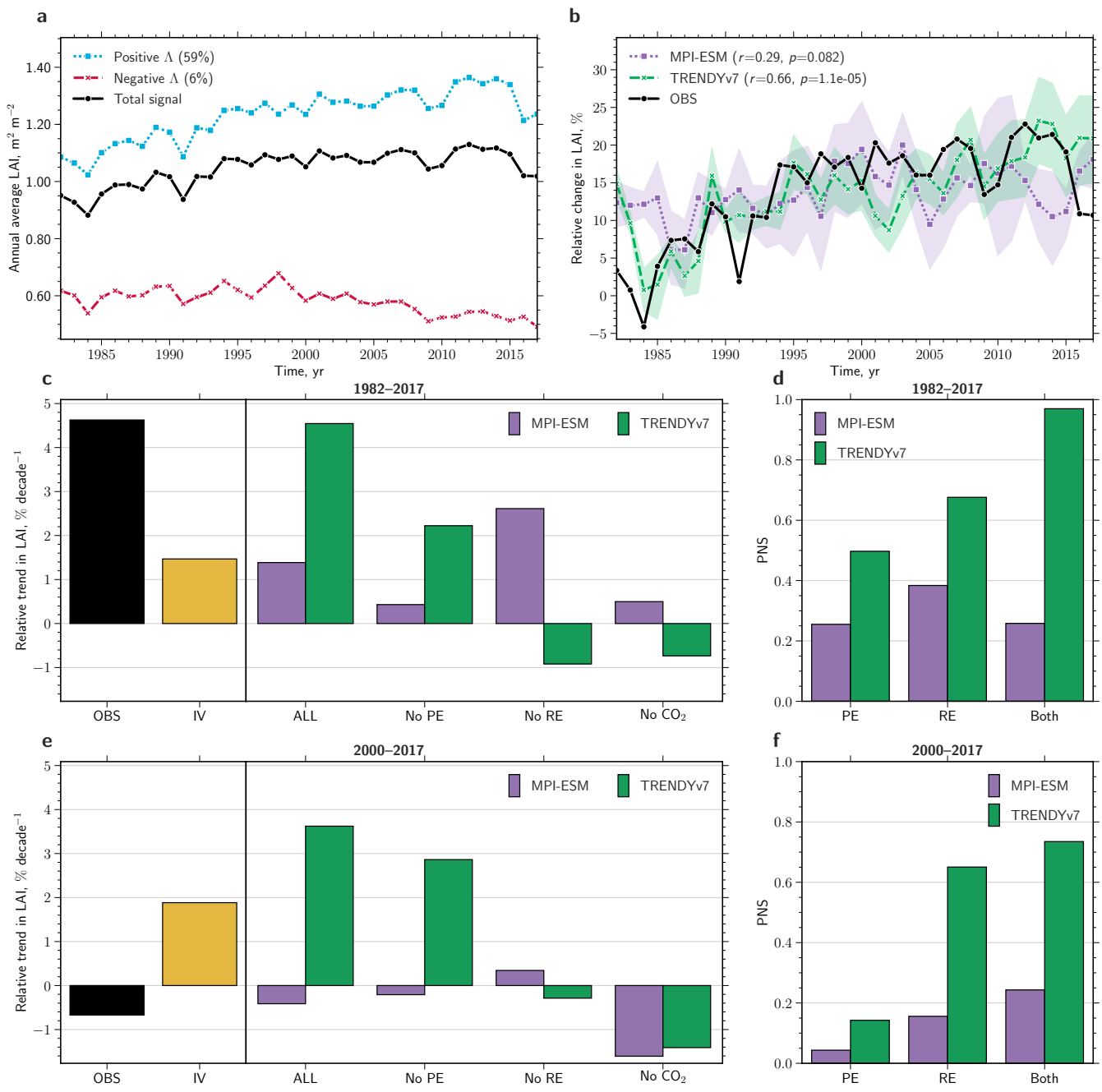


Fig. S13. Northern African Savannas Grasslands – caption analogous to Figure S4.

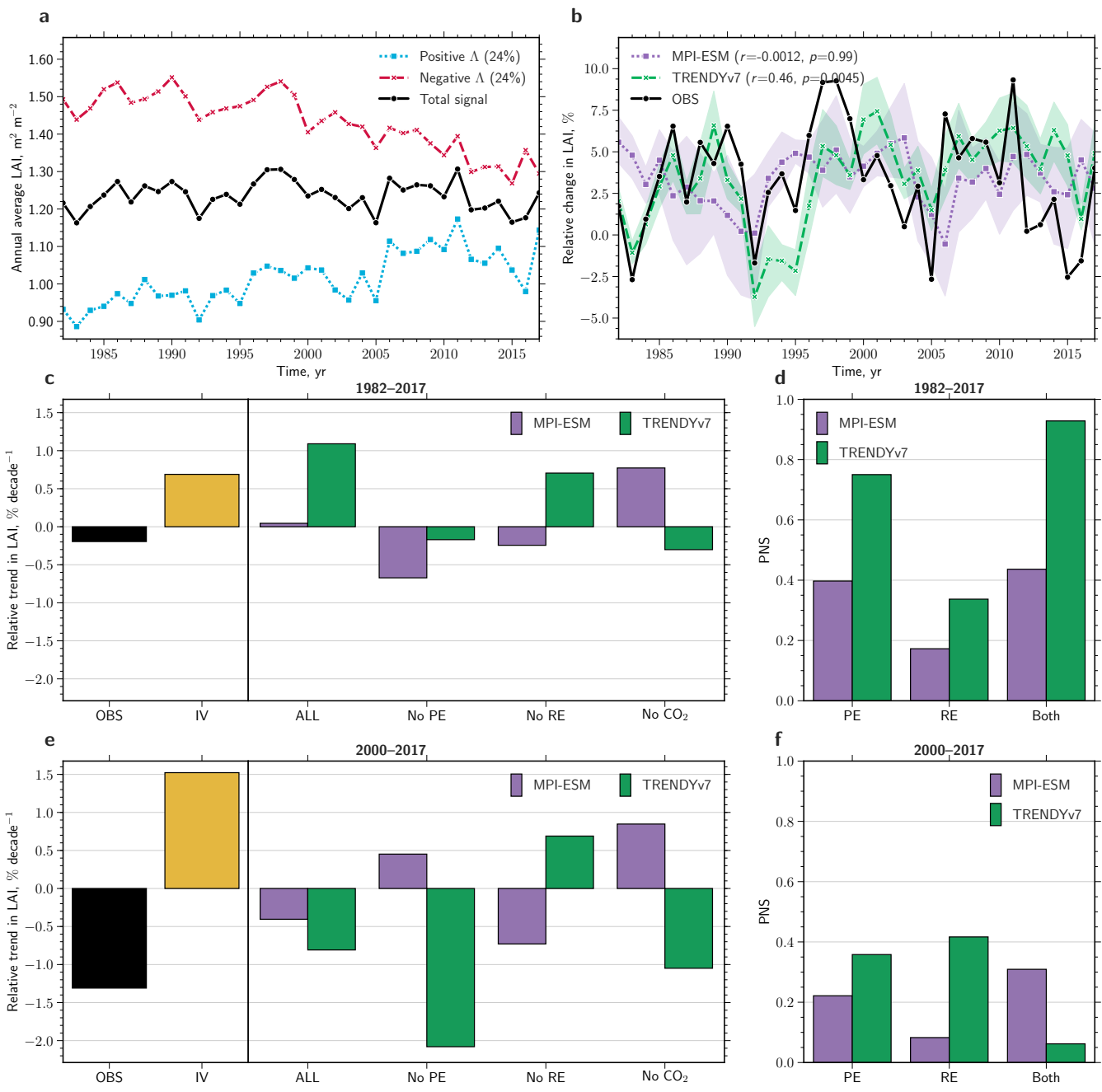


Fig. S14. Southern African Savannas Grasslands – caption analogous to Figure S4.

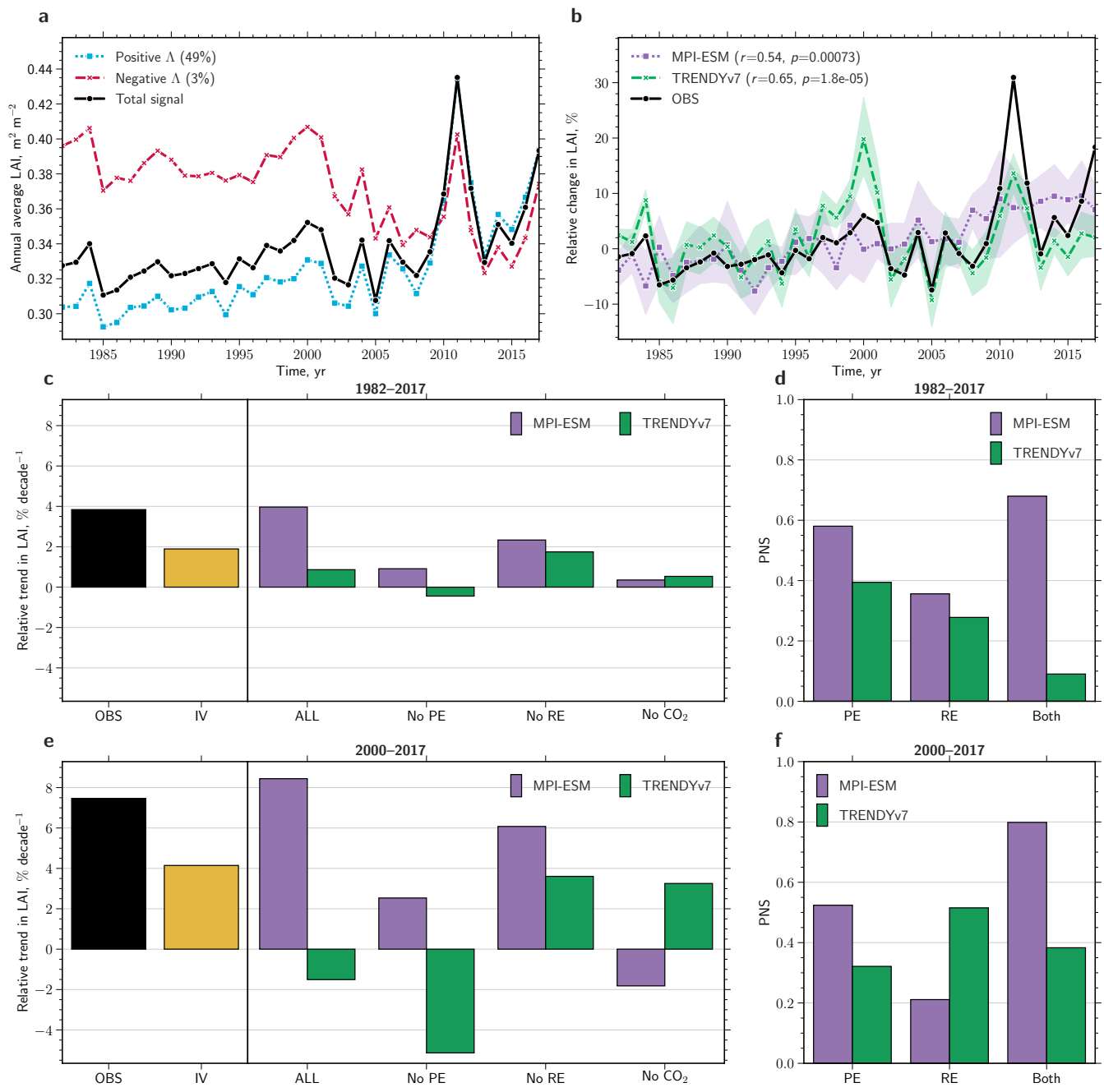


Fig. S15. Australian Shrublands – caption analogous to Figure S4.

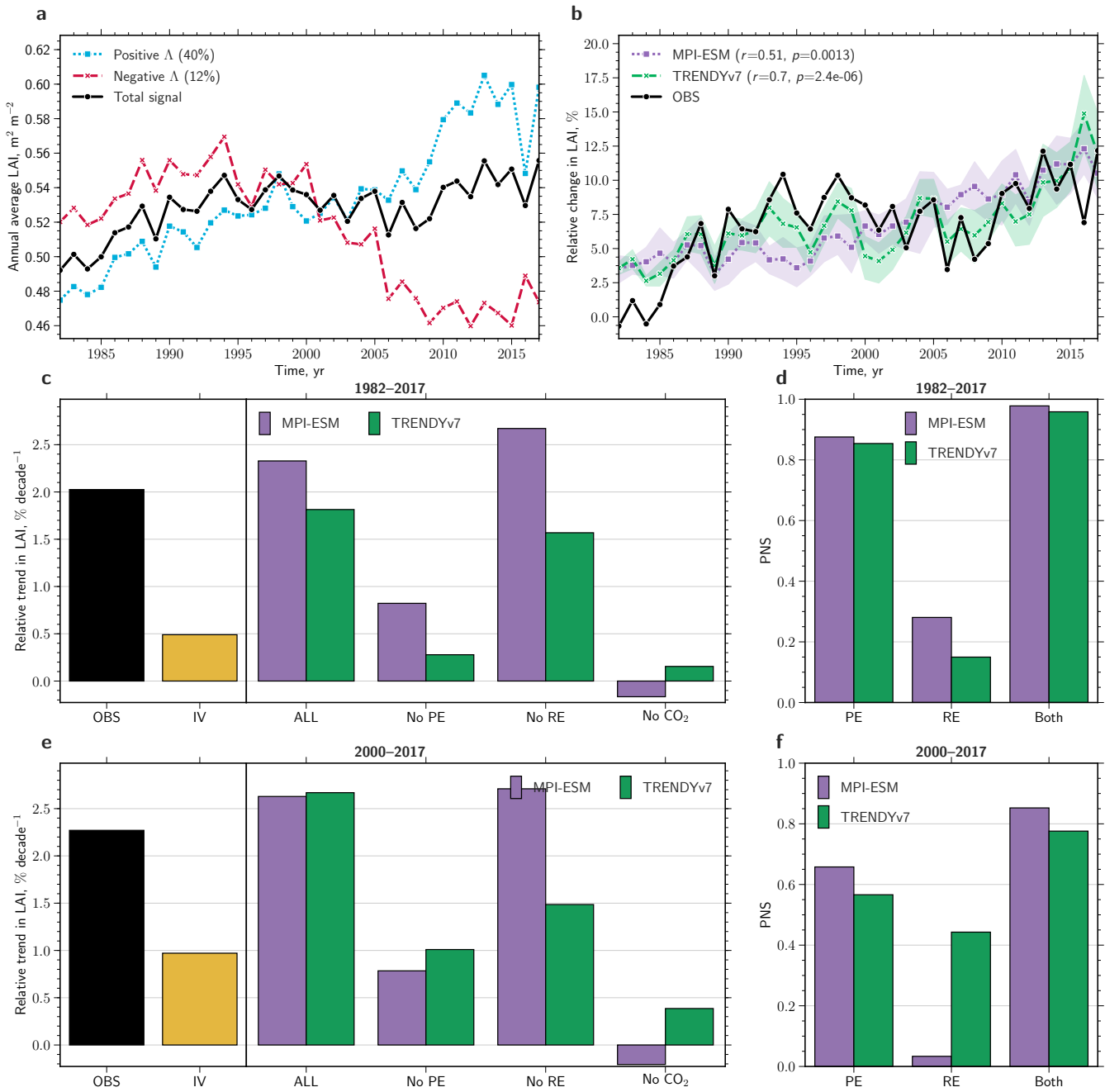


Fig. S16. Cool Grasslands – caption analogous to Figure S4.

Table S2. Greening (positive Δ), browning (negative Δ) and non-changing fractions of vegetated area for different biomes and prominent clusters of change for the time period 2000–2017. Significant changes are determined by the means of the Mann-Kendall significance test ($p < 0.1$). The abbreviations used to describe the different clusters are explained in Materials and Methods.

Area	Vegetated Area	Positive Δ Fraction	Negative Δ Fraction	No-Change Fraction
Unit	10^6 km^2	-	-	-
All Vegetation	109.42	0.21	0.13	0.66
Anthro. Vegetation	15.37	0.33	0.09	0.58
Natural Vegetation	94.05	0.19	0.14	0.68
Biomes				
Grasslands	26.77	0.22	0.12	0.66
Tropical F.	20.32	0.11	0.19	0.7
Boreal F.	13.69	0.19	0.18	0.63
Temperate F.	11.2	0.26	0.07	0.67
Shrublands	10.37	0.21	0.09	0.69
Tundra	7.03	0.14	0.14	0.72
Savannas	4.22	0.17	0.11	0.72
Clusters				
Cool Gl	12.32	0.26	0.12	0.62
EA Brl F	8.0	0.23	0.14	0.63
NAm Brl F	5.69	0.14	0.23	0.63
NAf Sv Gl	5.6	0.18	0.1	0.72
CAF Trp F	5.35	0.09	0.23	0.69
SAf Sv Gl	4.6	0.07	0.19	0.74
Aus Sl	4.43	0.29	0.02	0.69
EA Tundra	3.57	0.13	0.2	0.67
NAm Tundra	3.46	0.15	0.08	0.77

Table S3. Leaf area gain, loss, and net change for different biomes and prominent clusters of change for the time period 2000–2017. Significant changes are determined by the means of the Mann-Kendall significance test ($p < 0.1$). The abbreviations used to describe the different clusters are explained in Materials and Methods.

Leaf Area	Leaf Area Gain $10^3 \text{ km}^2 \text{ yr}^{-1}$	Leaf Area Loss $10^3 \text{ km}^2 \text{ yr}^{-1}$	Net Leaf Area Change $10^3 \text{ km}^2 \text{ yr}^{-1}$
<i>Unit</i>			
All Vegetation	140.25	-79.68	60.57
Anthro.Vegetation	40.69	-5.9	34.78
Natural Vegetation	99.56	-73.78	25.79
Biomes			
Grasslands	25.12	-11.65	13.47
Tropical F.	18.85	-37.27	-18.42
Boreal F.	15.02	-11.13	3.88
Temperate F.	26.29	-5.43	20.86
Shrublands	5.77	-1.85	3.91
Tundra	2.39	-2.68	-0.28
Savannas	5.97	-3.57	2.41
Clusters			
Cool Gl	10.23	-3.0	7.24
EA Brl F	11.82	-4.24	7.58
NAm Brl F	3.2	-6.9	-3.69
NAf Sv Gl	6.26	-1.25	5.01
CAF Trp F	3.5	-13.16	-9.66
SAF Sv Gl	1.52	-5.19	-3.67
Aus Sl	3.15	-0.12	3.02
EA Tundra	0.97	-2.23	-1.26
NAm Tundra	1.43	-0.45	0.97

11 References

- 12** 1. M. Rodell, P. R. Houser, U. Jambor, J. Gottschalck, K. Mitchell, C.-J. Meng, K. Arsenault, B. Cosgrove, J. Radakovich,
13 M. Bosilovich, J. K. Entin, J. P. Walker, D. Lohmann, and D. Toll. The Global Land Data Assimilation System. *Bulletin of the
14 American Meteorological Society*, 85(3):381–394, 2004. .
- 15** 2. D. P. Dee, S. M. Uppala, A. J. Simmons, P. Berrisford, P. Poli, S. Kobayashi, U. Andrae, M. A. Balmaseda, G. Balsamo, P. Bauer,
16 P. Bechtold, A. C. M. Beljaars, L. van de Berg, J. Bidlot, N. Bormann, C. Delsol, R. Dragani, M. Fuentes, A. J. Geer, L. Haimberger,
17 S. B. Healy, H. Hersbach, E. V. Hólm, L. Isaksen, P. Källberg, M. Köhler, M. Matricardi, A. P. McNally, B. M. Monge-Sanz,
18 J.-J. Morcrette, B.-K. Park, C. Peubey, P. de Rosnay, C. Tavolato, J.-N. Thépaut, and F. Vitart. The ERA-Interim reanalysis:
19 Configuration and performance of the data assimilation system. *Quarterly Journal of the Royal Meteorological Society*, 137(656):
20 553–597, 2011. .
- 21** 3. Miguel D. Mahecha, Fabian Gans, Gunnar Brandt, Rune Christiansen, Sarah E. Cornell, Normann Fomferra, Guido Kraemer,
22 Jonas Peters, Paul Bodesheim, Gustau Camps-Valls, Jonathan F. Donges, Wouter Dorigo, Lina M. Estupinan-Suarez, Victor H.
23 Gutierrez-Velez, Martin Gutwin, Martin Jung, Maria C. Londoño, Diego G. Miralles, Phillip Papastefanou, and Markus
24 Reichstein. Earth system data cubes unravel global multivariate dynamics. *Earth System Dynamics*, 11(1):201–234, 2020. .